How to Cite: Ergasheva, Kh.A., & Vokhidova, N.R. (2026). *Bombyx mori* Chitosan–Caffeine Nanocapsules: Formation, Structural Features, and Physicochemical Properties. *Eurasian Journal of Chemistry, 31, 1(121), 30–44*. https://doi.org/10.31489/2959-0663/1-26-2

Article

Received: 6 November 2025 | Revised: 26 February 2026 | Accepted: 2 March 2026 | Published online: 11 March 2026

UDC 541.64:547.458.6: 544.77.032.1

https://doi.org/10.31489/2959-0663/1-26-2

Khusnibonu A. Ergasheva*, Noira R. Vokhidova

Institute of Polymer Chemistry and Physics Academy of Sciences of Uzbekistan, Tashkent, Uzbekistan
*(*Corresponding author's e-mail: khusnibonu_ea@mail.ru)*

Bombyx mori Chitosan–Caffeine Nanocapsules: Formation, Structural Features, and Physicochemical Properties

This study aimed to engineer *Bombyx mori* chitosan–caffeine nanocapsules via a self-assembly approach and to comprehensively characterize their structural architecture, physicochemical properties, and release kinetics under precisely controlled pH conditions. Chitosan–caffeine nanocapsules were synthesized in aqueous medium at low temperature under controlled acidic conditions (pH 3.2 and 4.5), achieving yields of 91–94 %. Their physicochemical properties were analyzed using UV and FTIR spectroscopy, X-ray diffraction, scanning electron microscopy, and transmission electron microscopy. The results showed that hydrogen bonding and electrostatic interactions between the protonated amino groups of chitosan and the carbonyl groups of caffeine promoted the formation of spherical and oval nanostructures with diameters in the range of 100–400 nm. Spectroscopic analysis confirmed the intermolecular interactions responsible for encapsulation, while X-ray diffraction indicated a decrease in caffeine crystallinity after incorporation into the polymer matrix. SEM and TEM micrographs demonstrated efficient encapsulation of caffeine within the chitosan matrix and confirmed the formation of stable core–shell nanostructures. Release profile analysis showed that approximately 20 % of the total caffeine content was released from the chitosan nanocapsules over the monitored period, confirming their controlled release behavior. These chitosan-caffeine nanocapsules hold potential for future use in the development of drugs with prolonged release properties.

Keywords: chitosan, *Bombyx mori*, caffeine, nanoparticles, self-assembly, drug delivery systems, core–shell structures, controlled release

Introduction

Caffeine (CF, $C_8H_{10}N_4O_2$) is a biologically active compound widely used in pharmaceutical, nutraceutical, and cosmetic formulations due to its stimulant, antioxidant, and anti-inflammatory properties [1, 2]. However, its practical application is often limited by volatility, formulation-dependent solubility, local irritancy at elevated concentrations, and rapid diffusion in biological media. These factors are particularly critical in applications where stabilization and controlled release are required, such as topical, oral, and mucosal delivery systems [1–4].

Encapsulation into nanoscale carriers has been shown to improve caffeine stability, mask bitterness, and modulate release behavior [1–4]. Alongside polymeric nanoparticles and liposomal systems, supramolecular approaches based on cyclodextrins and calixarenes have also been reported to enhance caffeine performance through host–guest interactions [5, 6]. Nevertheless, multicomponent supramolecular systems often involve overlapping interaction mechanisms, which complicates the interpretation of structure–property relationships and limits systematic optimization [7, 8].

Chitosan (CS), a cationic polysaccharide obtained by deacetylation of chitin, is an attractive carrier owing to its biocompatibility, biodegradability, mucoadhesive properties, and suitability for controlled drug delivery [9–13]. Despite these advantages, chitosan-based systems face important challenges, including pH-dependent solubility, aggregation under physiological ionic strength, and limited retention of small, water-soluble molecules such as caffeine [14–17]. Various preparation techniques have been proposed, including ionic gelation, emulsification–crosslinking, and self-assembly, each yielding distinct structural and release characteristics [16, 18–23].

In the self-assembly approach, chitosan macromolecules interact with drug molecules under defined pH and ionic conditions, leading to the formation of nanocapsules in which the polymer constitutes the surrounding shell. Compared with other encapsulation techniques, self-assembly offers several advantages for chitosan–caffeine systems. The process is simple and environmentally friendly, as it does not require chemical crosslinkers or elevated temperatures, thereby preserving the chemical integrity and bioactivity of caf-

feine. The resulting nanocapsules are stabilized by natural intermolecular interactions, which promote structural stability and effective drug retention. In addition, the intrinsic affinity between chitosan and caffeine facilitates efficient drug loading, while modulation of formulation parameters enables control over capsule size and structural organization. Owing to these features, self-assembly is a suitable approach for the fabrication of chitosan–caffeine nanocapsules [20–22].

Chitosan–caffeine nanocapsules represent a promising platform for pharmaceutical delivery, and their modular nature allows the potential incorporation of additional bioactive components, such as vitamins, minerals, or polyphenols, to develop multifunctional systems [19–21]. Despite numerous studies on caffeine encapsulation using liposomes, nanoliposomes, and simple polymeric carriers, and reports showing that chitosan coating improves liposomal stability and mucoadhesion [23–28], several key limitations remain. Many studies rely on a single encapsulation strategy, such as chitosan-coated nanoliposomes or basic ionic-gelation particles, without systematically examining the influence of self-assembly parameters—particularly pH and chitosan-to-caffeine ratio—on caffeine stabilization. Furthermore, controlled-release claims are often not supported by detailed in vitro release analysis, and the physicochemical mechanisms governing the interaction of weakly basic molecules like caffeine with chitosan matrices are still insufficiently clarified. In addition, co-encapsulation of caffeine with other bioactive compounds in chitosan nanocapsules has been only rarely investigated with validated stability and release performance [29–37].

Based on the above, the aim of this study is to obtain nanocapsules based on chitosan *Bombyx mori* and caffeine by the "self-assembly" technique, as well as to study their morphology, physicochemical, and prolonged properties.

Experimental

Bombyx mori chitosan (CS) with a molecular mass (MM) of 84,000 and a deacetylation degree (DD) of 86 % was used, synthesized in laboratory conditions. Caffeine (CF) was purchased from China (CAS: 58-08-2). Additionally, 0.1 % analytical standard HCl and tetrahydrofuran (C_4H_8O) were used as the solvents. All the above, the reagents were AR grade.

Preparation of Chitosan-Caffeine Nanocapsules. To obtain chitosan-caffeine nanocapsules, a 1.0 % (w/v) solution of *Bombyx mori* chitosan in 0.1 N HCl and a 0.25 % (w/v) solution of CF in C_4H_8O were prepared. A homogeneous solution of chitosan was obtained at 25 ± 1 °C and continuous stirring at 500 rpm for ≈ 6 h. A 1 % (w/v) solution of caffeine in tetrahydrofuran (THF, C_4H_8O) was prepared for 50 min with vigorous stirring at 400 rpm. Nanocapsules were obtained at 35 ± 1 °C, 600 rpm for 1.5 h, and the mass ratios of the components were CS : CF = 1:0.3 and CS : CF = 1:0.03, respectively. The pH of the reaction mixture was adjusted to pH 3.2 ± 0.1 and pH 4.5 ± 0.1 using 0.1 N NaOH. Nanocapsule formation was induced by slowly adding 0.1 M Na_2SO_4 solution at a rate of 1 mL min^{-1}, which served as an ionic cross-linking and precipitating agent.

The suspension was then kept for 16 hours at 20 °C to achieve structural stabilization of the nanocapsules. The final product was separated by centrifugation for 10 min at 2000 rpm. The resulting powder was then repeatedly washed with bidistilled water to pH 7 and freeze-dried at –50 °C and 0.03 mbar (Christ Alpha 1-4 LDplus) for 24 hours to constant weight. All experiments were performed in triplicate to ensure reproducibility. Selected synthesis parameters, such as polymer concentration, mass ratio, pH, temperature, and stirring time, were optimized through preliminary screening to achieve encapsulation efficiency and obtain monodisperse nanoparticles. The results are presented in Table 1.

Table 1

Effect of pH and mass ratios of the initial reaction components on the production of CS-CF nanocapsules. τ = 1.5 h; v = 600 rpm

No	Designation in the text	Samples, mass ratio	pH	Reaction yield, %
1	Sample 1	CS-CF=1:0.3	3.2	91
2	Sample 2	CS-CF=1:0.3	4.5	94
3	Sample 3	CS-CF=1:0.03	4.5	92

Dynamic Light Scattering (DLS) Method. The size and distribution of particles in solutions were determined by dynamic light scattering (DLS) using a Photocor Compact-Z analyzer (Photocor Ltd., Moscow, Russia) equipped with a helium-neon laser operating at λ = 632.8 nm and 90° angle. The test solutions were

maintained at a thermostatted temperature of 25 ± 0.1 °C. The sample concentration was maintained at 0.05 mg/mL to minimize aggregation effects. Each measurement was performed for 3 minutes and repeated at least three times.

UV-Spectroscopic Studies. Measurements were performed on a SPECORD 210 spectrophotometer (Analytik Jena AG, Germany) in the wavelength range of 190–1000 nm with a 1 nm step and a scan rate of 2 nm/s. The accuracy of UV photometry was studied using potassium dichromate in accordance with the requirements of the European Pharmacopoeia, with an error of ±0.01. UV–Vis spectra were recorded in a quartz cuvette with an optical path length of 1 cm. Solutions of the studied samples were prepared in 2 % acetic acid, where the concentration was 0.002 mol/L. The pH of the reaction system was determined using a "pH-150".

Fourier Transform Infrared (FTIR) spectroscopy in the range of 400–4000 cm^{-1} using a Bruker INVENIO-S spectrophotometer (Bruker Optik GmbH, Ettlingen, Germany) was used to study the structure of the samples. Samples were prepared as tablets containing potassium bromide (150–250 mg KBr), and the solid sample (1.5–2 mg) was finely ground using a porcelain mortar. The sample mixture was placed in a mold and maintained under vacuum conditions, then pressed under a pressure of 7×10^8 Pa for 2 minutes.

X-Ray Diffraction (XRD) analysis of the samples was performed on a DRON-3M ("Burevestnik", St. Petersburg, Russia) X-ray diffractometer using monochromatic Co Kα radiation at 16 mA and 22 kV. Powdered samples were used for the study. The degree of crystallization (DC) of the samples was calculated by evaluating the intensity of the maximum diffraction curve based on the following formula:

$$DC = \frac{(I - I_a)i - K}{(I_c - I_a)i},$$

where, I_c and I_a are the intensities characteristic of the crystalline and amorphous regions, respectively [38].

Scanning Electron Microscope (SEM, JSM-IT 210, JEOL, Japan) was used to study the film morphology. During measurements, the accelerating voltage (EHT—Extra High Tension) was applied in the range of 5 kV to 15 kV, and the working distance was 10.8 mm. Images at various scales were obtained using InTouch Scope software. Energy dispersive spectroscopy (EDS) was used to determine the elemental composition of the synthesized samples, obtaining both spectra and elemental mapping images.

Transmission Electron Microscope (TEM, Talos F-200i from Thermo Fisher Scientific, USA)—a high-resolution TEM was used to determine nanoparticle sizes and film morphology. The voltage range was 20–200 kV. TEM images were obtained using samples deposited on standard carbon-coated copper grids.

In vitro Release Profile of Caffeine from Chitosan Nanocapsules (UV–Vis Spectroscopic Determination). The release profile of caffeine from chitosan nanocapsules was investigated using UV–spectrophotometry under *in vitro* conditions. CS-CF nanocapsules were prepared and suspended in an aqueous medium, and their release behavior was monitored over a specified period [39–45]. Release measurements were performed using a UV-Vis spectrophotometer with quartz cuvettes (optical path length of 1 cm). Absorption spectra were recorded in the wavelength range of 230–310 nm at selected time intervals (0, 900, 1800, 3600, 5400, 7200, and 9000 s). The analytical wavelength was set at the maximum of λ = 242 ± 2 nm, which corresponds to the characteristic absorption band of caffeine. At each time point, the average absorbance value was recorded on the display. To correct for background absorption, control spectra of a chitosan solution in 0.1 N HCl in the absence of caffeine were recorded under the same conditions. Corrected values were obtained by subtracting the control spectra from the spectra of the CS-CF sample, ensuring that the measured intensity reflects only caffeine release.

The corrected absorbance values at each time point were normalized to the value at the final time point (9000 s), which was defined as 100 % release. The cumulative release percentage (%R) was calculated using the following equation:

$$\%R(t) = \frac{A_t - A_{blank}}{A_{final} - A_{blank}} \times 100,$$

A_t is the absorbance at time t, A_{blank} is the absorbance of the blank solution, and A_{final} is the absorbance at the final time point (9000 s).

The release data were further analyzed using standard kinetic models. The Higuchi model was applied to evaluate diffusion-controlled release ($M_t/M_\infty = kH_t$), and the Korsmeyer–Peppas model ($M_t/M_\infty = k \cdot t^n$) was used to determine the release exponent n. An exponent value close to 0.5 indicates Fickian diffusion, while

higher values suggest anomalous (non-Fickian) transport. Regression fitting was performed to estimate kinetic parameters and interpret the release mechanism [39–45].

According to the *Higuchi model*, the release is proportional to the square root of time (t), which serves as the diffusion controller. The results deviate from the model at the initial points due to the "burst", but in the range of 1800–5400 s, they fit the Higuchi line relatively well. Also, according to the Korsmeyer–Peppas model, $M_t/M_\infty \approx k \cdot t^n$. If $n \approx 0.5 \rightarrow$ Fick diffusion; if $n > 0.5 \rightarrow$ anomalous (erosion + diffusion) mechanism. Accordingly, n is approximately in the range of 0.45–0.55, which indicates diffusion-controlled release [39, 40].

For statistical analysis of the experimental results, particle size and encapsulation efficiency measurements were performed in triplicate, and the results are expressed as mean ± standard deviation (SD). The statistical significance of differences between groups was assessed using a one-way analysis of variance (ANOVA) followed by a Tukey post-hoc test to determine pairwise differences between the different formulations. A significance level of $p < 0.05$ was considered statistically significant. This approach ensures the reliability and reproducibility of the obtained results, as is widely reported in nanomaterials and pharmaceutical research [46, 47].

Results and Discussion

Hydrodynamic Sizes of Chitosan–caffeine Samples

A suspension of the obtained CS-CF samples was prepared, and the hydrodynamic particle sizes were studied using DLS (Fig. 1).

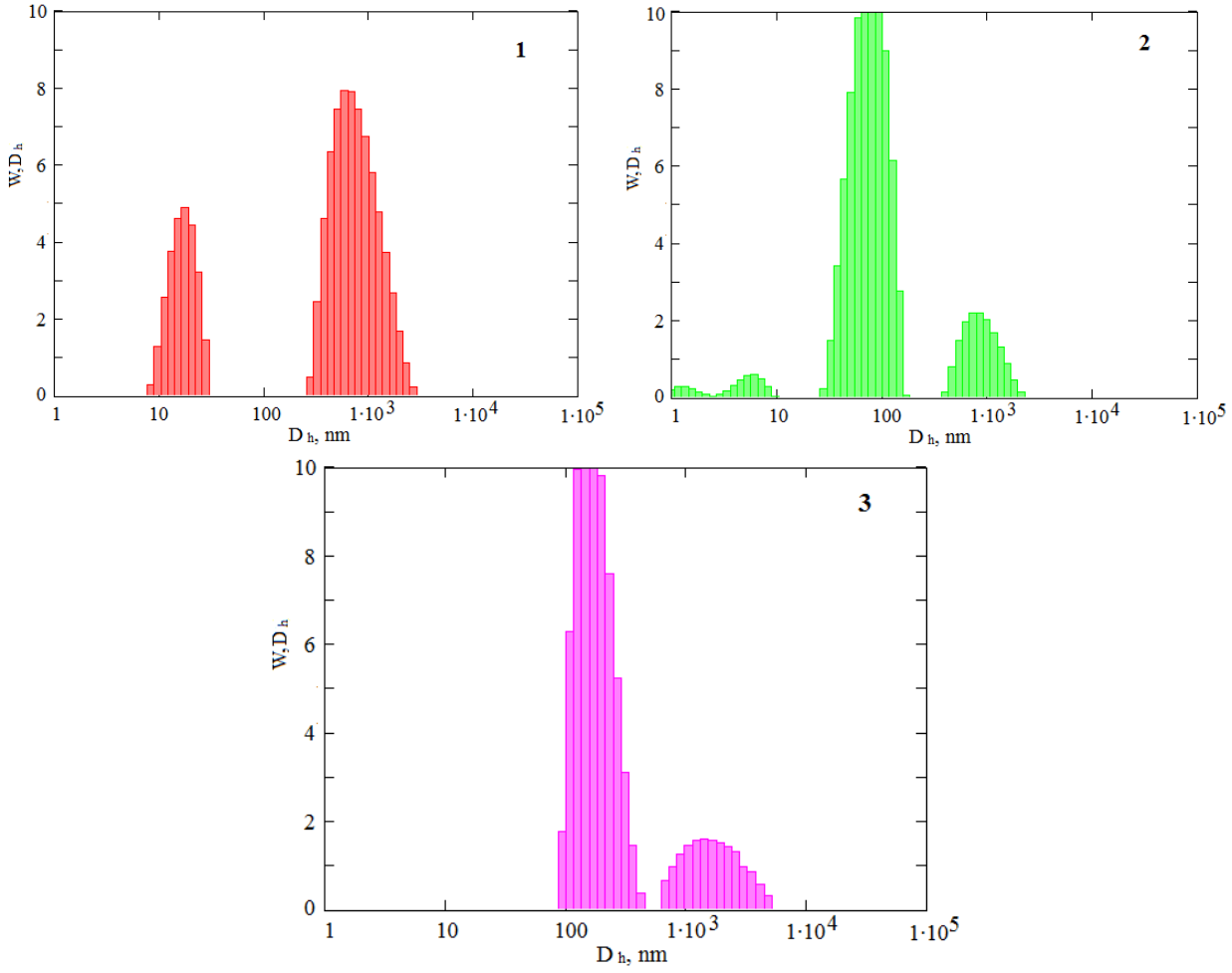

Figure 1. Hydrodynamic diameters and particle size distribution for samples of sample 1 (*1*), sample 2 (*2*), and sample 3 (*3*)

For samples 1 and 2, the predominant size range corresponded to average hydrodynamic diameters of 400–600 nm, while the histogram for sample 3 demonstrated comparatively larger particles with average sizes in the range of 500–700 nm. Overall, the results in Figure 1 demonstrate that the CS-CF samples exhibit a high degree of size polydispersity, ranging from approximately 20 nm to 1.5 μm. The polydispersity index (PDI) values ((Standard Deviation/Mean)²) are 0.580 for sample 1, 0.604 for sample 2, and 0.477 for sample 3 [48]. It appears that the formation of nanoparticles under the selected conditions for producing chitosan–caffeine nanocapsules is regulated by self-assembly mechanisms. That is, nanostructures are formed through electrostatic interactions between the protonated amino groups of chitosan and the polar regions of caffeine, supplemented by hydrogen bonds between the –NH groups of chitosan, as well as the C=O and heterocyclic –N atoms of caffeine. These non-covalent interactions promote the cooperative association of components, suppress the crystallization of caffeine, and stabilize the nanoscale structures.

UV-Spectroscopy

In spite of chitosan lacking a chromophore with high absorbance, its UV spectrum shows an absorption peak corresponding to π→π transitions in the range with a maximum at λ = 198–204 nm. In addition, a broad absorption band at λ = 280–310 nm is due to electronic transitions associated with amine and amide groups, as well as electronic transitions of conjugated structures (*n*→π*) [49]. In caffeine, the absorption band observed around 205 nm can be attributed to π→π* transitions associated with the conjugated ring system and carbonyl groups, while the band near 272 nm corresponds to n→π* transitions of the carbonyl moieties [50]. The expansion at 280–294 nm has been shown to be a result of their interaction with other molecules (Fig. 2) [51].

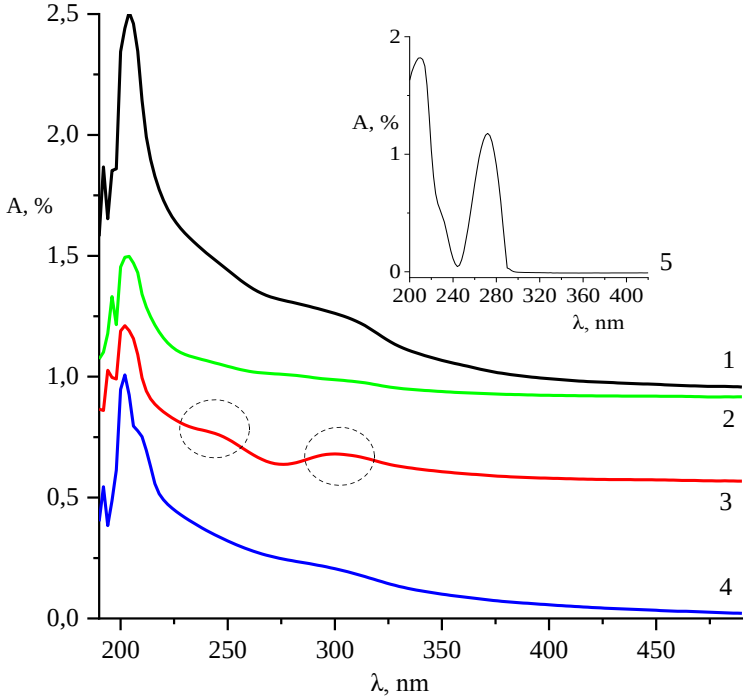

Figure 2. UV-spectra samples of chitosan (*1*); sample 1 (*2*); sample 2 (*3*); sample 3 (*4*), and caffeine samples (*5*)

The UV spectra of the chitosan–caffeine samples show the interaction of chitosan macromolecules with caffeine. The caffeine peak at λ = 266–273 nm is slightly shifted toward lower wavelengths, indicating the encapsulation of caffeine through the formation of hydrogen bonds ($–NH_3^+$ … O=C) between the protonated form of the amino groups of chitosan ($–NH_3^+$) and the carbonyl groups of caffeine (C=O) [52]. Such a bond partially "strains" the π-electron system of caffeine, and the energy required for electron transfer increases, which leads to a shift of λ_{max} toward shorter wavelengths. It is evident that an additional absorption band at 304 nm appears in the spectrum of sample 2, which is explained by the presence of conjugated structures in the chitosan molecule [53, 54]. Thus, the UV analysis confirms the encapsulation of caffeine in the chitosan matrix.

FTIR Spectroscopy

The IR spectrum of chitosan exhibits a broad absorption band at 3400–3200 cm^{-1}, which is associated with the stretching vibrations of hydroxyl (OH) and amino (NH) groups. The absorption band at 2920–2850 cm^{-1} corresponds to the stretching vibrations of CH in the aliphatic groups (CH, CH_2, CH_3) of chitosan. Vibrations in the absorption band at 1650–1600 cm^{-1} are very important and are related to the complex structure; in particular, the absorption band at 1600 cm^{-1} is characteristic of the stretching vibrations of the primary amine (NH_2). Stretching vibrations corresponding to C–N bonds were also observed at 1420 cm^{-1}, and deformation vibrations of –CH groups at 1380 cm^{-1}. The absorption band at 1150–1000 cm^{-1} is the "saccharide" absorption band, which corresponds to the stretching vibrations of glycosidic bonds. The absorption bands at 1070 cm^{-1} and 1030 cm^{-1} are characteristic of the C=O bond, and the absorption band at 1150 cm^{-1} is characteristic of the C–O–C bridge (Fig. 3, 1) [21, 49].

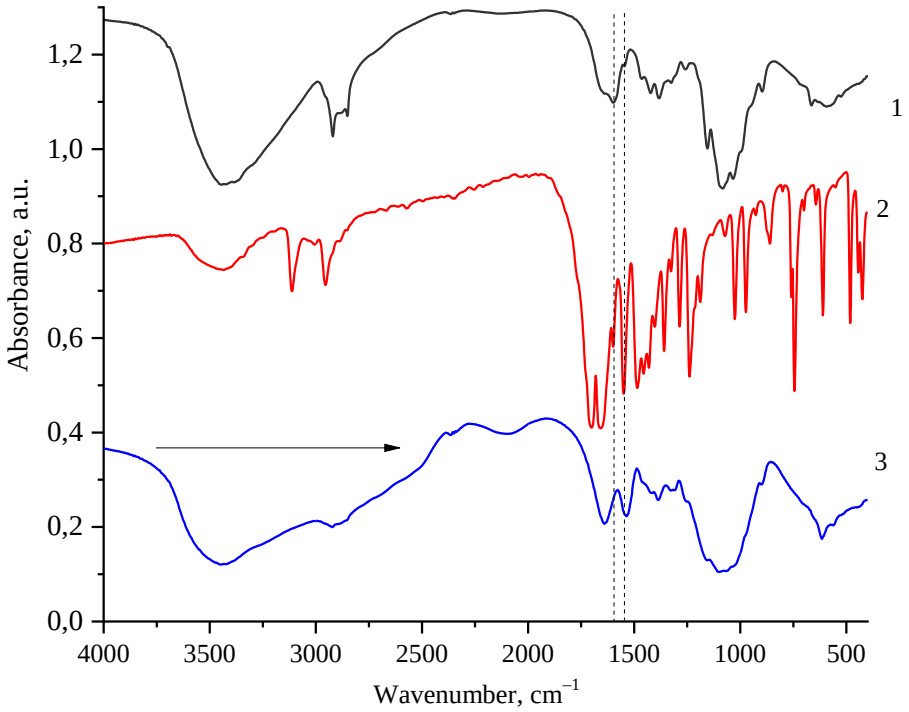

Figure 3. IR spectra of samples: chitosan (*1*), caffeine (*2*), and sample 2 (*3*)

The IR spectrum of caffeine displays CH stretching vibrations at 2950–2850 cm^{-1}, which are characteristic of the methyl groups attached to the nitrogen atoms in caffeine. These absorption bands are typically recorded in the spectrum of caffeine and are used to confirm the presence of methyl groups. The absorption bands at 1700 cm^{-1} and ~1650 cm^{-1} characterize C=O stretching vibrations of the carbonyl groups. Caffeine has two carbonyl groups, the exact position of which can vary slightly depending on the crystal form or environment. These carbonyl bands are considered the "fingerprint" of caffeine and are important for its identification. In addition, the absorption band in the 1550 cm^{-1} region is attributed to vibrations of the –C=N groups of the imidazole ring. The absorption bands at 1480 cm^{-1} and ~1450 cm^{-1} are characterized by C=C stretching vibrations of the aromatic ring and –CH bending vibrations of the methyl groups [55]. These peaks indicate the presence of a heterocyclic ring system in caffeine. The stretching vibrations at 1235 cm^{-1} are associated with –C=N bonds connecting the methyl groups to the nitrogen atoms in the ring. The region below 1200 cm^{-1} contains complex vibrations associated with –CN and C=O stretching, as well as ring deformations [56] (Fig. 3, 2).

The IR spectrum of sample 2 of CS-CF nanocapsules shows a broadening of the vibrational range of 3400–3200 cm^{-1}, characteristic of the –OH and –NH groups. The change in the width and intensity of this band indicates the interaction of chitosan with caffeine through their hydroxyl and amino groups. Also, a shift of the intense absorption band of the stretching vibrations of the amide I and amide II bonds of chitosan at 1640–1540 cm^{-1} is possibly associated with the interaction of caffeine with chitosan through hydrogen

bonds. Furthermore, due to a decrease in the intensity of the characteristic peaks of caffeine in CS-CF, it is assumed that under the chosen synthesis conditions, caffeine is encapsulated by chitosan [56–58] (Fig. 3, 3).

X-Ray Diffraction Patterns

X-ray diffraction study of the structure of caffeine reveals a high degree of crystallinity, which is reflected in its diffraction pattern by intense peaks at 2θ 11.79°; 12.43°; 20.88°; 23.66°; 24.01°; 26.14°; 26.38°; 26.79°; 27.02°; 28.35°; 29.49°; 30.26°; 36.36°; 38.06°; 39.01° and 39.58°, as well as other weak crystalline peaks (Fig. 4) [58, 59]. The size of caffeine single crystals at the indicated 2θ angles varied from 2 to 50 nm, averaging 25 nm. X-ray diffraction analysis of chitosan reveals that the polysaccharide has a semicrystalline structure. A weak diffraction peak at 2θ ≈ 10.4° indicates partial ordering of the chitosan chains, while a more pronounced peak at 2θ ≈ 19.95° is characteristic of the hydrated crystalline form of chitosan (MM 84 kDa; DD 86 %) (Fig. 4; line 3). These features are due to intra- and intermolecular hydrogen bonds in the polymer structure. The intensity and width of these peaks depend on factors such as the chitosan source, the degree of deacetylation, and processing conditions [60].

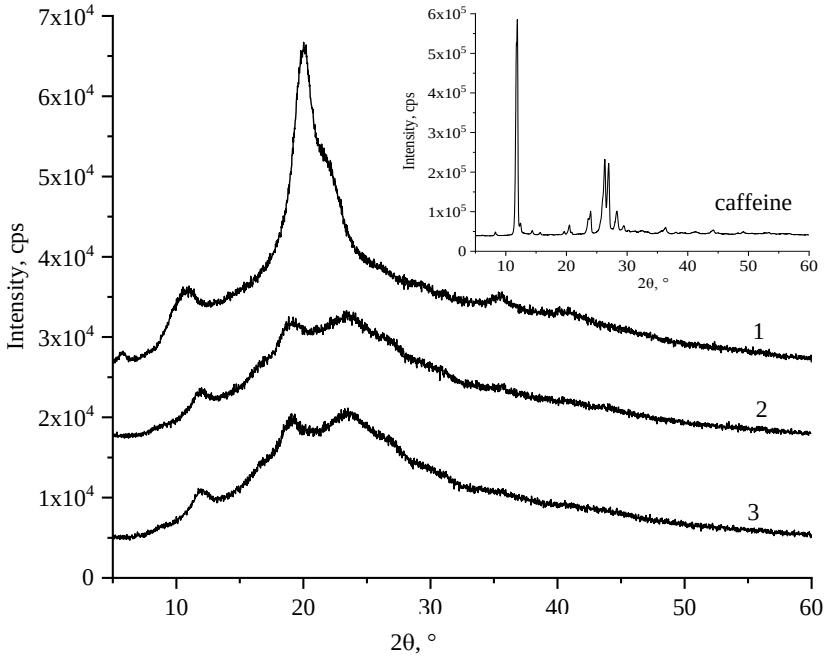

Figure 4. X-ray diffraction patterns of the sample 1 (*1*), sample 2 (*2*), and chitosan (*3*)

The X-ray diffraction patterns of the CS-CF nanocapsule samples differ significantly from those of the original CS and CF (Fig. 4; lines 1 and 2). It emerged that in the CS-CF samples, a shift in the characteristic crystalline peaks of CF at 2θ 11.8°, 18.7°, 23.1°, 35.8°, and 43.7° was observed, and the intensity of the characteristic peak associated with the semicrystalline structure of chitosan decreased, although it became broader. This behavior indicates a partial disruption of the semicrystalline structure of chitosan caused by its interaction with caffeine. The incorporation of caffeine molecules into the CS macromolecule disrupts the inter- and intramolecular hydrogen bonds between the chitosan chains, which leads to a decrease in crystallinity rather than to a complete destruction of the structure. At the same time, X-ray diffraction data indicate that the interaction is predominantly localized at the phase boundary, where the surface region of the caffeine core interacts with the surrounding chitosan shell, while some caffeine may retain residual crystalline order within the capsule. Shifts in the crystal peaks at 2θ further indicate interaction between caffeine and chitosan at the molecular level. The parameters of the crystalline unit cell of chitosan and nanocapsules were also calculated and are presented in Table 2.

Table 2

Crystal cell parameters of CS and CS-CF nanocapsules

No.	2θ, °	*d*, Å	(FWHM) β, °	(Size) L, nm
Chitosan				
1	10.49	8.43	2.54	3.28
2	19.95	4.44	1.98	4.3
CS-CF Sample 1				
3	11.89	7.44	1.41	5.93
4	18.73	4.735	2.02	4.17
5	23.17	4.01	2.9	3
6	35.82	2.505	0.75	11.7
7	43.75	2.067	1.3	6. 8
CS-CF Sample 2				
8	11.92	7.42	1.62	5.13
9	18.96	4.677	1.43	5.9
10	23.17	4.01	2.9	2.9
11	35.23	2.545	3.3	2.6
12	44.5	2.03	3.6	2.5

The sample 2 nanocapsules showed that it has a monoclinic type crystal structure: *a* — 7.211 Å, *b* — 2.806 Å, *c* — 9.305 Å; α — 90º, β — 90º, γ — 90º. Thus, the monoclinic structure provides insights into the stability of the nanocapsules, which is important for their application in drug delivery.

Scanning Electron Microscope (SEM) Results

A SEM image of chitosan demonstrates that it has a generally porous, loose structure with numerous irregularities and channels. A scale estimate shows that the large particles have a diameter of approximately 1–5 μm. Within these structures, the presence of smaller structures, possibly in the range of 100–300 nm, can be predicted (Fig. 5). The particles are round or oval in shape, indicating possible self-assembly. Some areas appear as denser aggregates, which may indicate partial agglomeration of the particles. On the whole, the structure appears well-distributed, without large clumps, indicating a stable distribution of the components [61, 62].

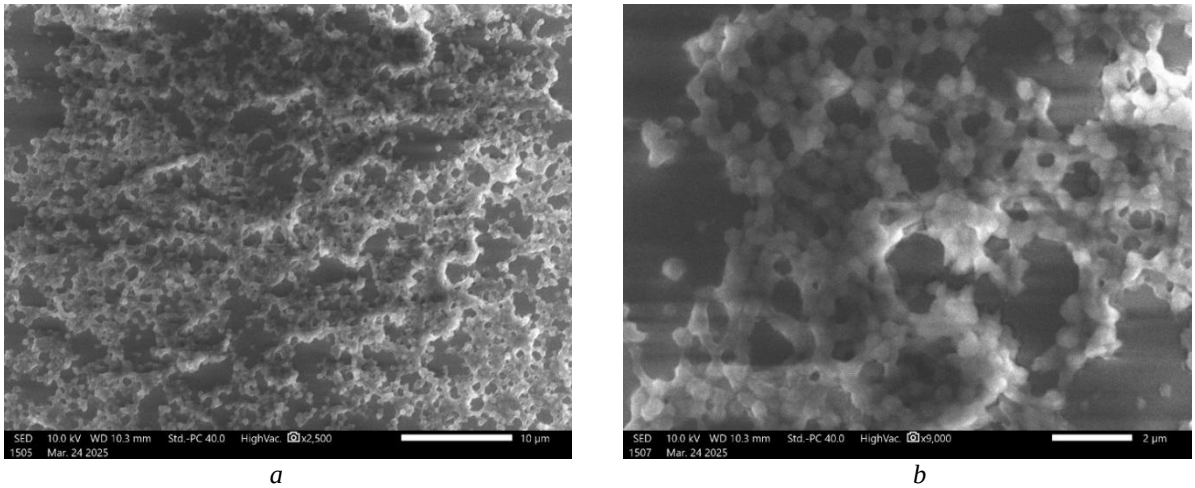

a *b*

Figure 5. SEM micrographs of the surface morphology of chitosan: *a* — ×10 μm; *b* — ×2 μm

SEM micrographs reveal elongated, needle-like structures (Fig. 6), which are characteristic of crystalline caffeine morphology reported in previous studies [63].

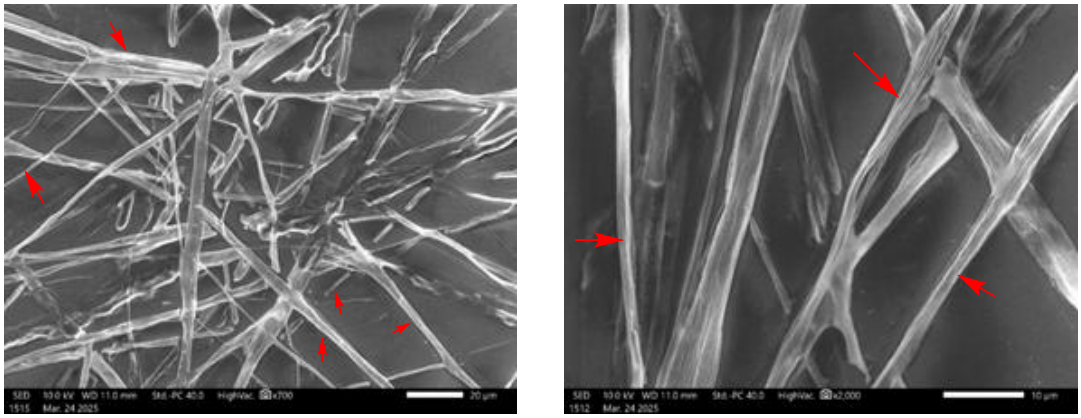

a *b*

Figure 6. SEM micrographs of the surface morphology of caffeine: *a* — ×20 μm; *b* — ×10 μm

Figures 7–9 show the SEM micrographs obtained according to Table 1. The results indicate that the morphology of the nanocapsules depends significantly on the pH of the synthesis and the ratio of chitosan to caffeine. From Figure 7, it is evident that the morphology of sample 1 CS-CF formed particles of different sizes, approximately from 224 nm to 448 nm, within which spherical nanoparticles can be distinguished, indicating a controlled self-assembly and encapsulation process. The spherical morphology is typical of chitosan-based nanocarriers formed through ionic gelation or polyelectrolyte complexation, and similar features have been noted for caffeine-loaded chitosan nanocapsules [2, 21].

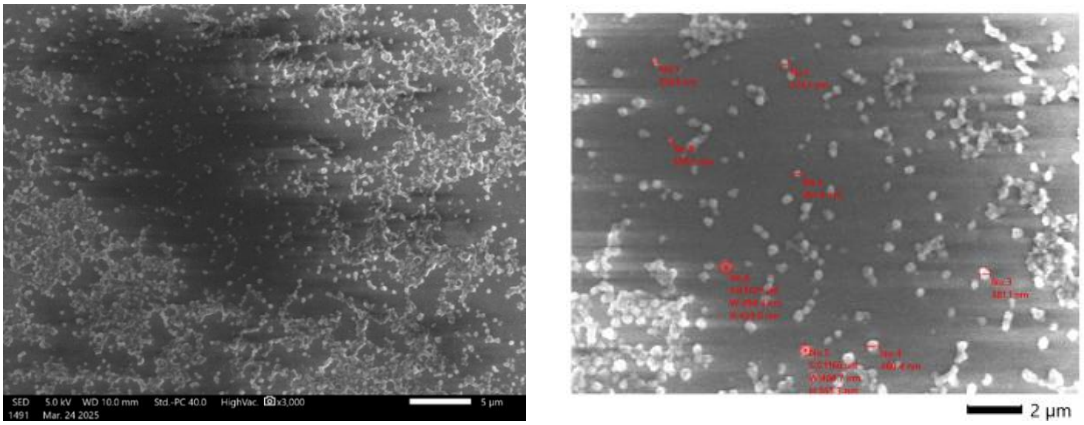

a *b*

Figure 7. SEM micrographs of the surface morphology of sample 1: *a* — ×5 μm; *b* — ×2 μm

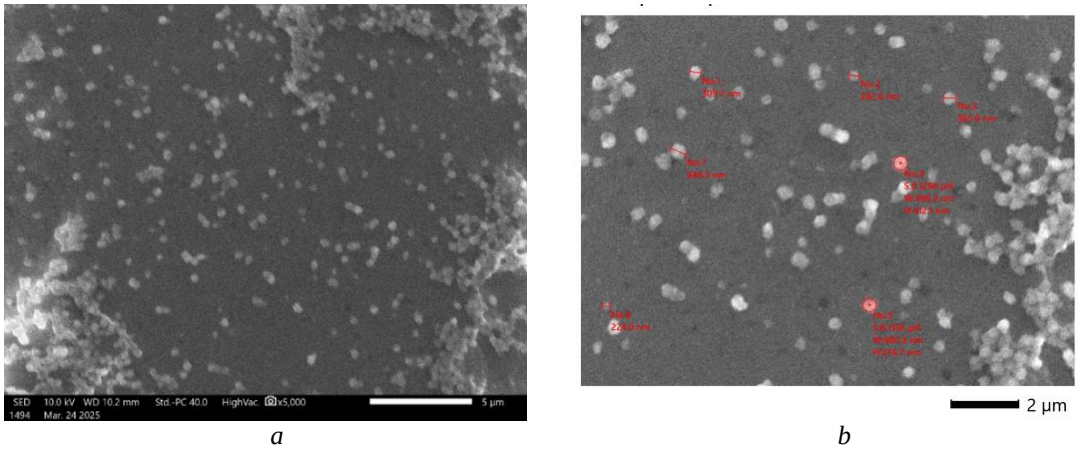

a *b*

Figure 8. SEM micrographs of the surface morphology of sample 2: *a* —×5 μm; *b* — ×2 μm

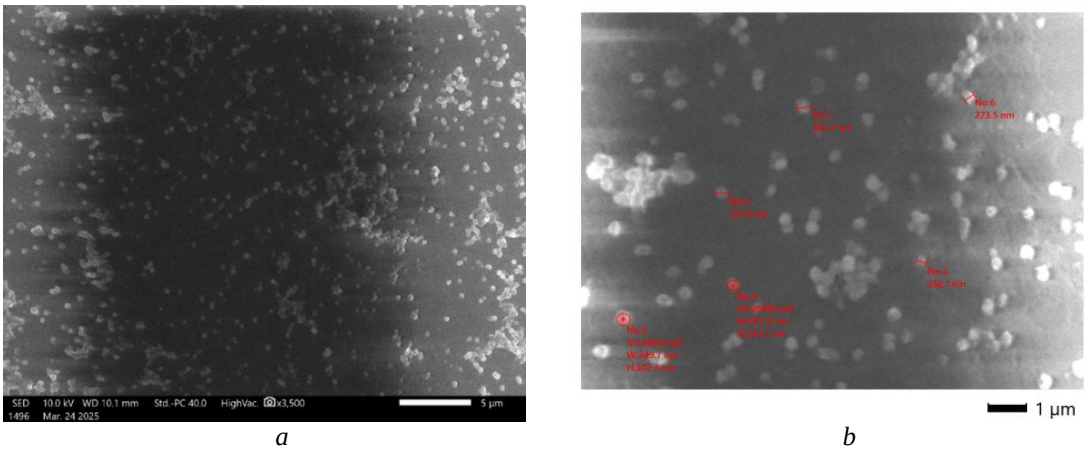

a *b*

Figure 9. SEM micrographs of the surface morphology of sample 3: *a* — ×5 μm; *b* — ×1 μm

It should be emphasized that pH adjustment changes the degree of protonation of chitosan and thus controls the balance between intermolecular attraction and repulsion. After particle formation, the residual positive surface charge of chitosan creates electrostatic repulsion between particles, limiting uncontrolled aggregation and ensuring the formation of stable, self-assembling spherical nanocapsules.

As evidenced by Figure 8, the surface morphology of sample 2 nanocapsules is similar to that of sample 1. Particle size varies: for example, one is approximately 365 nm long, while another is approximately 224 nm, and some are even larger, reaching 448 nm. Surface area (S) and height (H) measurements were taken, indicating the three-dimensional characteristics of the particles.

Results from surface morphology studies of sample 3 show that the largest particles are approximately 120 nm and 116 nm in size (Fig. 9). Smaller particles, approximately 71 nm and 28.4 nm in size, are also present. It is noteworthy that the particles have different sizes and shapes, which may indicate their complex morphology. The difference in size may indicate the presence of aggregates or individual nanoparticles.

Thus, it was demonstrated that the resulting nanocapsules have a distinctive surface morphology compared to the original components. It was found that encapsulating caffeine with chitosan macromolecules results in particles that differ from chitosan and caffeine in both size and shape.

Transmission Electron Microscope (TEM) Results

TEM images of nanocapsules—sample 1 and sample 2 show the presence of capsule-shaped particles with overall dimensions of approximately 215 nm (Fig. 10). In both cases, these particles are surrounded by a shell with a characteristic thickness in the range of approximately 150–200 nm, indicating the formation of well-developed capsule structures. The similarity of the characteristic dimensions confirms the reproducibility of nanocapsule size under different synthesis conditions, while variations in shell thickness reflect differences in the degree of chitosan precipitation and structural compaction.

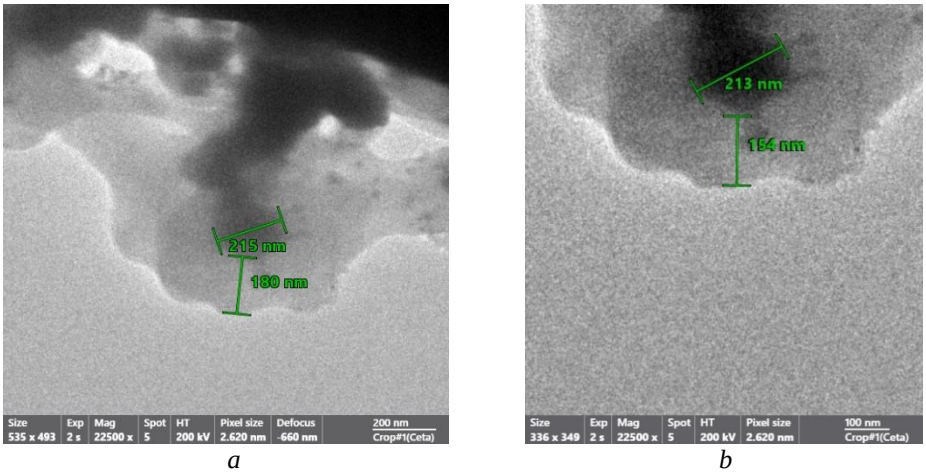

a *b*

Figure 10. TEM images of sample 1 (*a*) and sample 2 (*b*)

The microphotograph of sample 3 shows nanostructures. In the center and left are two particles, 120 nm and 116 nm in size, respectively. Smaller particles extending from them are 71 nm, 51.3 nm, and 28.4 nm. Overall, the images show nanostructures with the expected particle sizes (Fig. 11*a*). Figure 11*b* shows a particle with a length of 81 nm, likely corresponding to a small region or thickness of part of the structure. 107 nm is another measured dimension, possibly the length or width of a particular part. 264 nm and 265 nm are two very similar dimensions that may indicate the width or extent of different parts of the object. The overall scale of the image is 200 nm, indicating that all measurements refer to tiny structures, likely on the micro- or nanoscale (Fig. 11*b*).

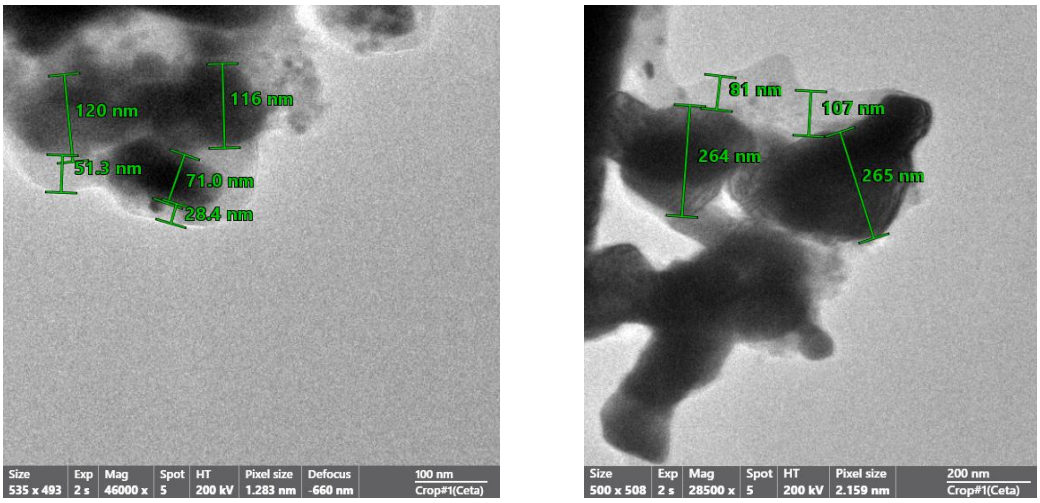

a *b*

Figure 11. TEM images of chitosan-caffeine sample 3

The results of SEM and TEM studies confirm the formation of predominantly spherical and oval chitosan-caffeine nanocapsules. SEM micrographs revealed well-dispersed nanoparticles with a smooth surface and minimal agglomeration, indicating a uniform morphology. TEM images further demonstrate that caffeine was effectively encapsulated within the chitosan matrix, forming core-shell nanostructures with a clear contrast between the polymer shell and the encapsulated core. These results confirm the efficient encapsulation and stable morphology of the synthesized nanocapsules [2, 21].

Controlled Release of Caffeine

Controlled release of caffeine is essential for increasing the bioavailability of drugs and reducing side effects. The results obtained show that at 900 s, $\lambda \approx 242$ nm, A = 1.455 (maximum); thereafter, the peak intensity decreased and stabilized in the range of A = 1.12–1.21 from 3600 to 9000 s. The spectral shift: λ_{peak} gradually shifted from 242 nm → 236 nm. This hypsochromic shift indicates that the microenvironment surrounding caffeine (pH, interaction with the polymer) is changing (Fig. 12).

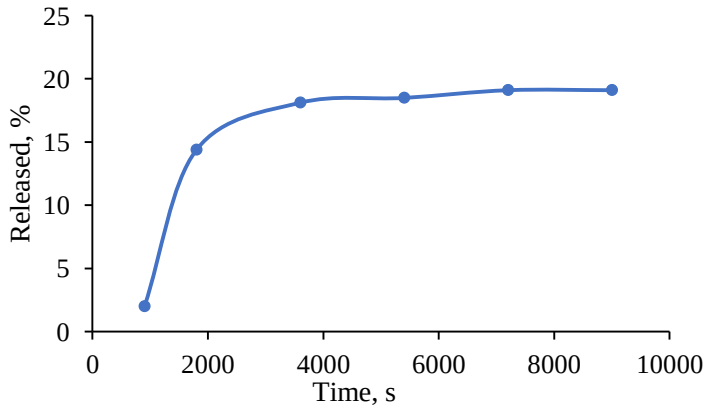

Figure 12. Dependence of the percentage of caffeine release from chitosan nanocapsules on time

Figure 12 manifests that the relatively high intensity in the initial stages of prolongation compared to the final stage indicates that the majority of the caffeine is quickly released from the capsule at 900 s of the process. In other words, a "burst" release is observed. This is explained by the rapid diffusion of caffeine molecules near the surface. Subsequently, the caffeine within the matrix is gradually released, providing a prolonged release phase. Comparison of the obtained results reveals a shift in the λ peaks and an initial high intensity of chitosan capsules in the matrix-solvent medium. This is due to the fact that she protonated amino groups of chitosan interact with caffeine molecules through ionic and hydrogen bonds. Over time, these bonds weaken, and the caffeine is released. Therefore, an initial rapid release (burst) occurs, followed by a slow release phase controlled by diffusion. A biphasic release profile is advantageous in pharmaceuticals, since the first phase provides a rapid therapeutic effect, while the second phase maintains a stable concentration over an extended period (Fig. 12) [64–67]. In conclusion, the release of caffeine from chitosan-caffeine nanocapsules is a two-stage process: Rapid release (~900 s) and diffusion-controlled extended release (1800–9000 s) are observed. The shift in the λ peak confirms the change in the caffeine microenvironment within the chitosan matrix. The kinetic analysis is consistent with the Higuchi and Korsmeyer–Peppas models, indicating that the release occurs predominantly through Fickian diffusion. This profile confirms the potential of chitosan-caffeine nanocapsules as a drug delivery system with rapid and extended release.

Conclusions

The study demonstrated that the formation of chitosan–caffeine nanocapsules is strongly influenced by both the pH of the reaction medium and the mass ratio of the components. Under the selected conditions (pH 3.2 and 4.5), the reaction yields reached 91–94 %, confirming the efficiency of the applied synthesis approach. DLS analysis revealed hydrodynamic particle sizes predominantly in the 400–700 nm range with polydispersity indices of 0.477–0.604, indicating the formation of heterogeneous but stable nanoscale dispersions. UV–Vis spectroscopy showed a hypsochromic shift of the characteristic caffeine absorption band, confirming intermolecular interactions within the polymer matrix. FTIR spectra demonstrated broadening and shifts in the –OH/–NH and amide regions, supporting the formation of hydrogen bonding between chitosan and caffeine. XRD patterns indicated a decrease in the crystallinity of caffeine after encapsulation, reflecting disruption of its ordered structure within the composite system. SEM micrographs revealed predominantly spherical and oval particles with average sizes of approximately 220–450 nm for samples synthesized at higher caffeine ratios and 30–120 nm for the lower-ratio system. TEM analysis further confirmed discrete nanocapsules with characteristic dimensions around 200–400 nm, supporting the formation of structurally organized polymer–drug assemblies distinct from the initial components. The release profile showed that the cumulative percentage of caffeine released from chitosan nanocapsules reached approximately 20 % over the monitored time period. These results collectively confirm the successful formation of chitosan–caffeine nanocapsules and substantiate their potential for controlled drug delivery applications.

Funding

This study was conducted with the basic funding of the Academy of Sciences of the Republic of Uzbekistan.

*Author Information**

**The authors' names are presented in the following order: First Name, Middle Name and Last Name*

Khusnibonu Abdukayum kizi Ergasheva (*corresponding author*) — Junior Researcher, Institute of Polymer Chemistry and Physics, 100128; e-mail: khusnibonu_ea@mail.ru; https://orcid.org/0009-0006-9418-2491

Noira Rahimovna Vokhidova — Doctor of Chemical Sciences, Professor, Head of the Laboratory of Interpolyelectrolyte Complexes and Metallopolymers, Institute of Polymer Chemistry and Physics, 100128, Tashkent, Uzbekistan; e-mail: noira_vokhidova@yahoo.de; https://orcid.org/0000-0003-0477-3708

Author Contributions

The manuscript was written through the contributions of all authors. All authors have given approval to the final version of the manuscript. CRediT: **Khusnibonu Abdukayum kizi Ergasheva** investigation, validation, writing-original draft; formal analysis, editing; **Noira Rahimovna Vokhidova** conceptualization, data curation, formal analysis, validation & editing.

Acknowledgment

The authors acknowledge the staff of the Laboratory of Chemical and physico-chemical research methods at the Institute of Chemistry and Physics of Polymers, in particular candidate of physical and mathematical sciences N.S. Ashurov and junior researcher S. Shakhobiddinov, for their valuable assistance in the interpretation of UV spectroscopy and DLS measurement results.

Conflicts of Interest

The authors declare no conflict of interest

References

1 Abdoli, F., Davoudi, M., Momeni, F., et al. (2024). Estimate the prevalence of daily caffeine consumption, caffeine use disorder, caffeine withdrawal, and perceived harm in Iran: a cross-sectional study. *Scientific Reports*, 14, 7644. https://doi.org/10.1038/s41598-024-58496-8

2 Seyedabadi, M. M., Rostami, H., Jafari, S. M., & Fathi, M. (2021). Development and characterization of chitosan-coated nanoliposomes for encapsulation of caffeine. *Food Bioscience*, 40, 100857. https://doi.org/10.1016/j.fbio.2020.100857

3 Peng, H., Brown, M., Bowdler, P., & Honeychurch, K. C. (2020). Extraction-free, direct determination of caffeine in microliter volumes of beverages by thermal desorption–gas chromatography–mass spectrometry. *International Journal of Analytical Chemistry*, 2020, 5405184. https://doi.org/10.1155/2020/5405184

4 Chow, C. H., Kan, Y. C., & Ho, K. S. (2019). A simple and rapid gas chromatographic method for routine caffeine determination in beverages using a nitrogen–phosphorus detector. *Journal of Analytical Chemistry*, 74, 764–770. https://doi.org/10.1134/S1061934819080045

5 Radeva, L., Kalampalika, E., Yordanov, Y., Petrov, P. D., Tzankova, V., & Yoncheva, K. (2025). Formulation of caffeine–hydroxypropyl-β-cyclodextrin complex in hydrogel for skin treatment. *Gels*, 11, 326. https://doi.org/10.3390/gels11050326

6 Kashapov, R. R., Kashapova, N. E., Ziganshina, A. Y., Syakaev, V. V., Khutoryanskiy, V. V., & Zakharova, L. Y. (2021). Interaction of mucin with viologen and acetate derivatives of calix[4]resorcinols. *Colloids and Surfaces B: Biointerfaces*, 208, 112089. https://doi.org/10.1016/j.colsurfb.2021.112089

7 Chen, X.-M., Chen, Y., Hou, X.-F., Wu, X., Gu, B.-H., & Liu, Y. (2018). Sulfonato-β-cyclodextrin mediated supramolecular nanoparticle for controlled release of berberine. *ACS Applied Materials & Interfaces*, 10, 25555–25563. https://doi.org/10.1021/acsami.8b08651

8 Schneider, H.-J. (2009). Binding mechanisms in supramolecular complexes. *Angewandte Chemie International Edition*, *48*(22), 3924–3977. https://doi.org/10.1002/anie.200802947

9 Ibrahim, A. G., Elgammal, W. E., & Hassan, S. M. (2024). Development of a chitosan derivative bearing the thiadiazole moiety and evaluation of its antifungal and larvicidal efficacy. *Polymer Bulletin*, 81(2), 1291–1302. https://doi.org/10.1007/s00289-023-04765-x

10 Naskar, S., Sharma, S., & Kuotsu, K. (2019). Chitosan-based nanoparticles: An overview of biomedical applications and their preparation. *Journal of Drug Delivery Science and Technology*, 49, 66–81. https://doi.org/10.1016/j.jddst.2018.10.022

11 Duan, C., Meng, X., Meng, J., et al. (2019). Chitosan as a preservative for fruits and vegetables: a review on chemistry and antimicrobial properties. *Journal of Bioresources and Bioproducts*, 4, 11–21. https://doi.org/10.21967/jbb.v4i1.189

12 Fouda, M. M., Wittke, R., Knittel, D., & Schollmeyer, E. (2009). Use of chitosan/polyamine biopolymers based on cotton as a model system to prepare antimicrobial wound dressing. *International Journal of Diabetes Mellitus*, 1, 61–64. https://doi.org/10.1016/j.ijdm.2009.05.005

13 Shaban, N. Z., Aboelsaad, A. M., Shoueir, K. R., et al. (2020). Chitosan-based dithiophenolato nanoparticles: preparation, mechanistic information of DNA binding, antibacterial, and cytotoxic activities. *Journal of Molecular Liquids*, 318, 114252. https://doi.org/10.1016/j.molliq.2020.114252

14 Kou, W., Yang, Y., Fan, H., et al. (2024). Regeneration of dental pulp via collagen hydrogel composited with resveratrol-loaded chitosan nanoparticle in a rabbit model of dental pulp injury. *Polymer Bulletin*, 81, 14235–14248. https://doi.org/10.1007/s00289-024-05318-6

15 Zakharova, N. V., Simonova, M. A., Zelinskii, S. N., et al. (2019). Synthesis, molecular characteristics, and stimulus-sensitivity of graft copolymer of chitosan and poly(N,N-diethylacrylamide). *Journal of Molecular Liquids*, 292, 111355. https://doi.org/10.1016/j.molliq.2019.111355

16 Hu, T., Ma, Y., Huang, J., et al. (2020). Self-organized thermo-responsive poly(lactic-co-glycolic acid)-graft-pullulan nanoparticles for synergistic thermo-chemotherapy of tumor. *Carbohydrate Polymers*, 237, 116104. https://doi.org/10.1016/j.carbpol.2020.116104

17 Roy, H., Nayak, B. S., & Nandy, S. (2020). Chitosan-anchored nanoparticles in current drug development utilizing computer-aided pharmacokinetic modeling: Case studies for target-specific cancer treatment and future perspectives. *Current Pharmaceutical Design*, 26, 1666–1675. https://doi.org/10.2174/1381612826666200203121241

18 Khan, M. M., Madni, A., Torchilin, W., et al. (2019). Lipid–chitosan hybrid nanoparticles for controlled delivery of cisplatin. *Drug Delivery*, 26, 765–772. https://doi.org/10.1080/10717544.2019.1642420

19 Francescato, G., Leitão, M. I. P. S., Orsini, G., & Petronilho, A. (2024). Synthesis and medicinal applications of N-heterocyclic carbene complexes based on caffeine and others. *ChemMedChem*, 19, e202400118. https://doi.org/10.1002/cmdc.202400118

20 Lessa, E. F., Nunes, M. L., & Fajardo, A. R. (2018). Chitosan/waste coffee-grounds composite: An efficient and eco-friendly adsorbent for removal of pharmaceutical contaminants from water. *Carbohydrate Polymers*, 189, 257–266. https://doi.org/10.1016/j.carbpol.2018.02.018

21 Mehrabi-Khozani, Z., Jafari, S. M., Sarabandi, K., Rezaei, A., & Maghsoudlou, Y. (2024). Stabilization of caffeine-loaded nanoliposomes via chitosan coating and spray drying for food product applications. *Carbohydrate Polymer Technologies and Applications*, 8, 100617. https://doi.org/10.1016/j.carpta.2024.100617

22 Xu, Y., Kim, C. S., Saylor, D. M., & Koo, D. (2017). Polymer degradation and drug delivery in PLGA-based drug–polymer applications: A review of experiments and theories. *Journal of Biomedical Materials Research Part B: Applied Biomaterials, 105*(6), 1692–1716. https://doi.org/10.1002/jbm.b.33648

23 Zhang, H., Oh, M., Allen, C., & Kumacheva, E. (2020). Monodisperse chitosan nanoparticles for mucosal drug delivery. *Biomacromolecules, 21*(6), 2244–2252. https://doi.org/10.1021/bm0496211

24 Alvarez-Lorenzo, C., & Concheiro, A. (2014). Smart drug delivery systems: From fundamentals to the clinic. *Chemical Communications*, 50, 7743–7765. https://doi.org/10.1039/C4CC01429D

25 Song, X., Singh, M., Lee, K. E., Vinayagam, R., & Kang, S. G. (2024). Caffeine: A Multifunctional Efficacious Molecule with Diverse Health Implications and Emerging Delivery Systems. *International Journal of Molecular Sciences*, 25(22), 12003. https://doi.org/10.3390/ijms252212003

26 Paul, B., Xie, L., Yahia, Z. O., & Chen, W. (2025). Recent Review on the Stability of Bioactive Substances Through Encapsulation and Their Application in Dairy Products. *Food Reviews International*, 42(2), 605–631. https://doi.org/10.1080/87559129.2025.2492338

27 Layek, B., & Das, S. (2021). Chitosan-based nanomaterials in drug delivery applications. *Biopolymer-Based Nanomaterials in Drug Delivery and Biomedical Applications*, 185–219. https://doi.org/10.1016/b978-0-12-820874-8.00001-4

28 Mohammed, M. A., Syeda, J. T. M., Wasan, K. M., & Wasan, E. K. (2017). An overview of chitosan nanoparticles and their application in non-parenteral drug delivery. *Pharmaceutics, 9*(4), 53. https://doi.org/10.3390/pharmaceutics9040053

29 Grierosu, C., Calin, G., Damir, D., Marcu, C., Cernei, R., Zegan, G., Anistoroaei, D., Moscu, M., Carausu, E. M., Duceac, L. D., Dabija, M. G., Mitrea, G., Gutu, C., Bogdan Goroftei, E. R., & Eva, L. (2023). Development and Functionalization of a Novel Chitosan-Based Nanosystem for Enhanced Drug Delivery. *Journal of Functional Biomaterials*, 14(11), 538. https://doi.org/10.3390/jfb14110538

30 Martins, A. F., Facchi, S. P., Follmann, H. D., et al. (2014). Antimicrobial activity of chitosan derivatives containing N-quaternized moieties in its backbone: A review. *International Journal of Molecular Sciences, 15*(11), 20800–20832. https://doi.org/10.3390/ijms151120800

31 Jiménez-Gómez, C. P., & Cecilia, J. A. (2020). Chitosan: A natural biopolymer with a wide and varied range of applications. *Molecules, 25*(17), 3981. https://doi.org/10.3390/molecules25173981

32 Agnihotri, S. A., Mallikarjuna, N. N., & Aminabhavi, T. M. (2004). Recent advances in chitosan-based micro- and nanoparticles for drug delivery. *Journal of Controlled Release, 100*(1), 5–28. https://doi.org/10.1016/j.jconrel.2004.08.010

33 Illum, L. (1998). Chitosan and its use as a pharmaceutical excipient. *Pharmaceutical Research, 15*(9), 1326–1331. https://doi.org/10.1023/A:1011929016601

34 Elsabee, M. Z., & Abdou, E. S. (2013). Chitosan-based edible films and coatings: A review. *Materials Science and Engineering C, 33*(4), 1819–1841. https://doi.org/10.1016/j.msec.2013.01.010

35 Sogias, I. A., Williams, A. C., & Khutoryanskiy, V. V. (2008). Why is chitosan mucoadhesive? *Biomacromolecules, 9*(7), 1837–1842. https://doi.org/10.1021/bm800276d

36 Bernkop-Schnürch, A., & Dünnhaupt, S. (2012). Chitosan-based drug delivery systems. *European Journal of Pharmaceutics and Biopharmaceutics, 81*(3), 463–469. https://doi.org/10.1016/j.ejpb.2012.04.007

37 Kean, T., & Thanou, M. (2010). Biodegradation, biodistribution, and toxicity of chitosan. *Advanced Drug Delivery Reviews, 62*(1), 3–11. https://doi.org/10.1016/j.addr.2009.09.004

38 Wunderlich, B. (2002). The measurement of the crystallinity of polymers by DSC. *Polymer*, 43, 3873–3878. https://doi.org/10.1016/S0032-3861(02)00235-5

39 Van Bavel, N., Issler, T., Pang, L., Anikovskiy, M., & Prenner, E. J. (2023). A Simple Method for Synthesis of Chitosan Nanoparticles with Ionic Gelation and Homogenization. *Molecules*, 28(11), 4328. https://doi.org/10.3390/molecules28114328

40 Zaman, M., Butt, M. H., Siddique, W., Iqbal, M. O., Nisar, N., Mumtaz, A., Nazeer, H. Y., Alshammari, A., & Riaz, M. S. (2022). Fabrication of PEGylated Chitosan Nanoparticles Containing Tenofovir Alafenamide: Synthesis and Characterization. *Molecules*, 27(23), 8401. https://doi.org/10.3390/molecules27238401

41 Jafernik, K., Kaczmarek, M., Buta, M., et al. (2023). Chitosan-based nanoparticles as effective drug delivery systems: A review. *Molecules, 28*(4), 1963. https://doi.org/10.3390/molecules28041963

42 Borges, M. M. C., Teixeira, H. F., & Sousa, J. J. (2025). Controlled release of perillyl alcohol via pH-responsive polymeric carriers: Fitting to Korsmeyer–Peppas model. *ACS Omega*, 10, 1–11. https://doi.org/10.1021/acsomega.5c04817

43 El-Naggar, N. E. A., Shiha, A. M., Mahrous, H., et al. (2022). Green synthesis of chitosan nanoparticles, optimization, and characterization against biofilms. *Scientific Reports*, 12, 19869. https://doi.org/10.1038/s41598-022-24303-5

44 Gutiérrez-Ruiz, S. C., Cortés, H., González-Torres, M., et al. (2024). Optimize the parameters for synthesis by ionic gelation, purification, and freeze-drying of chitosan-TPP nanoparticles for biomedical applications. *Journal of Biological Engineering*, 18, 12. https://doi.org/10.1186/s13036-024-00403-w

45 Yuan, Q., Shah, J., Hein, S., & Misra, R. D. K. (2010). Controlled and extended drug release behavior of chitosan-based nanoparticle carrier. *Acta Biomaterialia, 6*(3), 1140–1148. https://doi.org/10.1016/j.actbio.2009.08.027

46 Conte, R., De Luca, I., Valentino, A., Cerruti, P., Pedram, P., Cabrera-Barjas, G., Moeini, A., & Calarco, A. (2023). Hyaluronic Acid Hydrogel Containing Resveratrol-Loaded Chitosan Nanoparticles as an Adjuvant in Atopic Dermatitis Treatment. *Journal of Functional Biomaterials, 14*(2), 82. https://doi.org/10.3390/jfb14020082

47 Martín-Escaño, A., Barbuzano, C., Rodríguez-Díaz, J. M., & Pérez-Herrero, E. (2026). Statistical optimization of chitosan-based synthesis strategies to generate albumin nanoparticles. *Drug Delivery and Translational Research*. https://doi.org/10.1007/s13346-026-02046-4

48 Filippov, S. K., Khusnutdinov, R., Murmiliuk, A., Inam, W., Zakharova, L. Ya., Zhang, H., & Khutoryanskiy, V. V. (2023). Dynamic light scattering and transmission electron microscopy in drug delivery: A roadmap for correct characterization of nanoparticles and interpretation of results. *Materials Horizons*, 10, 5354–5370. https://doi.org/10.1039/d3mh00717k

49 Kumirska, J., Czerwicka, M., Kaczynski, Z., et al. (2010). Application of spectroscopic methods for structural analysis of chitin and chitosan. *Marine Drugs, 8*(5), 1567–1636. https://doi.org/10.3390/md8051567

50 Gayathri, G., D'Souza, J. Q., & Sundaram, N. G. (2023). UV induced photocatalytic degradation of caffeine using TiO_2–H-beta zeolite composite. *Minerals, 13*(4), 465. https://doi.org/10.3390/min13040465

51 Bhawani, S. A., Fong, S. S., & Ibrahim, M. N. M. (2015). Spectrophotometric analysis of caffeine. *International Journal of Analytical Chemistry*, 2015, 170239. https://doi.org/10.1155/2015/170239

52 Herdiana, Y., Wathoni, N., Shamsuddin, S., & Muchtaridi, M. (2022). Drug release study of the chitosan-based nanoparticles. *Heliyon, 8*(1), e08674. https://doi.org/10.1016/j.heliyon.2021.e08674

53 Meynaud, S., Huet, G., Brulé, D., Gardrat, C., Poinssot, B., & Coma, V. (2023). Impact of UV irradiation on the chitosan bioactivity for biopesticide applications. *Molecules, 28*(13), 4954. https://doi.org/10.3390/molecules28134954

54 Edwards, A. A., & Alexander, B. D. (2010). Organic applications of UV–visible absorption spectroscopy. In *Encyclopedia of Spectroscopy and Spectrometry* (2nd ed., pp. 2030–2039). https://doi.org/10.1016/B978-0-12-374413-5.00013-0

55 Rajam, K., et al. (2013). Effect of caffeine–Zn^{2+} system in preventing corrosion of carbon steel in well water. *Journal of Chemistry*, 2013, 521951. https://doi.org/10.1155/2013/521951

56 Hamed, A., Ghareeb, D., Mohamed, T. M., Hamed, M., Nofal, M. S., & Gaber, M. (2023). Caffeine–folic acid-loaded chitosan nanoparticles combined with methotrexate as a novel HepG2 immunotherapy targeting adenosine A_2A receptor downstream cascade. *BMC Complementary Medicine and Therapies*, 23, 384. https://doi.org/10.1186/s12906-023-04212-4

57 Stefanowska, K., Woźniak, M., Majka, J., Sip, A., Mrówczyńska, L., Kozak, W., Dobrucka, R., & Ratajczak, I. (2023). Chitosan Films with Caffeine and Propolis as Promising and Ecofriendly Packaging Materials. *Applied Sciences, 13*(22), 12351. https://doi.org/10.3390/app132212351

58 Woźniak, M., Gromadzka, K., & Kwaśniewska-Sip, P. (2022). Chitosan–caffeine formulation as an ecological preservative in wood protection. *Wood Science and Technology*, 56, 1851–1867. https://doi.org/10.1007/s00226-022-01426-6

59 Kamburova, K., Boshkova, N., Radeva, T., Shipochka, M., & Boshkov, N. (2024). Chitosan–alginate nanocontainers with caffeine as green corrosion inhibitors for the protection of galvanized steel. *Crystals, 14*(7), 660. https://doi.org/10.3390/cryst14070660

60 Lehmann, R., & Stowasser, K. (2007). The crystal structure of anhydrous beta-caffeine as determined from X-ray powder-diffraction data. *Chemistry — A European Journal, 13*(10), 2908–2911. https://doi.org/10.1002/chem.200600973

61 Affes, S., Aranaz, I., Acosta Contreras, F. N., & Heras, Á. (2022). Physicochemical and biological properties of chitosan derivatives with varying molecular weight produced by chemical depolymerization. *Biomass Conversion and Biorefinery, 14*(3), 1–11. https://doi.org/10.1007/s13399-022-02662-3

62 Song, W., Zhang, Q., Guan, Y., Li, W., Xie, S., Tong, J., Li, M., & Ren, L. (2022). Synthesis and characterization of porous chitosan/saccharomycetes adsorption microspheres. *Polymers, 14*(11), 2292. https://doi.org/10.3390/polym14112292

63 Khanmohammadi, M., Elmizadeh, H., & Ghasemi, K. (2015). Investigation of the size and morphology of chitosan nanoparticles used in a drug delivery system employing chemometric techniques. *Iranian Journal of Pharmaceutical Research, 14*(3), e125312. https://doi.org/10.22037/ijpr.2015.1761

64 Sarfraz, A., Simo, A., Fenger, R., Christen, W., Rademann, K., Panne, U., & Emmerling, F. (2012). Morphological diversity of caffeine on surfaces: Needles and hexagons. *Crystal Growth & Design, 12*, 583–588. https://doi.org/10.1021/cg101358q

65 Milkova, V., & Goycoolea, F. M. (2020). Encapsulation of caffeine in polysaccharide oil-core nanocapsules. *Colloid and Polymer Science*, 298(8), 1035–1041. https://doi.org/10.1007/s00396-020-04653-0

66 Dash, M., Chiellini, F., Ottenbrite, R. M., & Chiellini, E. (2011). Chitosan — A versatile semi-synthetic polymer in biomedical applications. *Progress in Polymer Science, 36*(8), 981–1014. https://doi.org/10.1016/j.progpolymsci.2011.02.001

67 Naskar, S., Kuotsu, K., & Sharma, S. (2018). Chitosan-based nanoparticles as drug delivery systems: a review on two decades of research. *Journal of Drug Targeting*, 27(4), 379–393. https://doi.org/10.1080/1061186x.2018.1512112